3. Chapter 3

Results

Molecular modeling

Docking of CAII reference ligands with Autodock

Human CA II, is one of the most commonly studied enzymes with 279 X-ray crystallographic structures and a wealth of information regarding various inhibitors of CAII (235). Tuccinardi *et al.* (2007) determined via cross-docking analysis using the ChemScore GOLD docking program that the 1okn, 1kwr, 1cim, 1bnw, 1cnx, 1oq5 and 1ttm X-ray structures displayed the best RMSD average of the redocked ligands (193). These receptors were chosen to be employed in the study as part of an ensemble docking study. Ligands extracted from 52 human CAII X-ray structures were redocked into the selected receptors and the best score of each ligand was chosen (Table 3.1). The correlationbetween the calculated Autodock 4.0 free energy of binding ($AD4_{\epsilon}$) and the experimentally determinedinhibition constant ($expK_i$) as well as the root mean squared deviation (RMSD) of the docked ligandcompared to the X-ray structure were calculated.

A coefficient of determination (R^2) 0.5856 between $expK_i$ and $AD4_{\epsilon}$is given with the following logarithmicfunction (Figure 3.1):

$$AD4_{\epsilon} = 0.144\ln(expK_i) - 9.809$$

This result indicatesthat the docking software is able to at least differentiate between µM and nM active compounds (Table 3.1, Figure 3.1).

Table 3.1: Best docking energy of redocked CAII ligands.Ligands were docked into1okn, 1kwr, 1cim, 1bnw, 1cnx, 1oq5 and 1ttm X-ray structures.

	RCSB PDB accession code	expK$_i$- nM (reference)	Autodock 4.0 docking energy (AD4$_€$) (kcal/mol)	RMSD Å
1	**2nng**	8200(236)	-8.01	1.67
2	**3bet**	1500(237)	-9.45	1.02
3	**1okm**	1450(238)	-8.72	2.86
4	**1okl**	930(238)	-8.82	0.42
5	**2nns**	900(236)	-8.78	2.01
6	**2h15**	640(239)	-9.29	1.78
7	**2nn1**	400(236)	-9.11	1.18
8	**1xq0**	137(240)	-8.89	2.32
9	**2pov**	75(241)	-8.93	0.69
10	**1z9y**	65(235)	-9.36	1.98
11	**2pow**	63(241)	-9.06	2.83
12	**1ttm**	45(242)	-9.57	1.69
13	**2aw1**	43(243)	-9.6	2.03
14	**2pou**	38(241)	-9.19	0.52
15	**1eou**	36(244)	-9.37	1.97
16	**2hl4**	30(245)	-9.39	2.07
17	**1xpz**	27(240)	-9.46	2.61
18	**1oq5**	21(246)	-9.58	0.68
19	**1ze8**	21(247)	-9.24	1.34
20	**2hd6**	16(248)	-9.26	2.64
21	**3daz**	11.8(195)	-8.58	2.41
22	**1kwq**	9.21(249)	-9.49	1.77
23	**3d8w**	7.00 (195)	-9.11	0.97
24	**2q1q**	7.00 (250)	-8.95	2.61
25	**1kwr**	6.61(249)	-9.36	1.89
26	**3hku**	5.00 (251)	-9.83	1.99

27	**1a42**	3.2(252)	-8.96	0.85
28	**3d9z**	2.00 (195)	-9.44	1.82
29	**1cin**	1.9(253)	-9.95	0.81
30	**1bnv**	1.7(254)	-9.98	0.83
31	**1cim**	1.5(253)	-9.62	0.67
32	**1g54**	1.5(255)	-8.88	1.07
33	**1i90**	1.28(256)	-9.74	3.62
34	**1i8z**	1.27(256)	-10.08	0.98
35	**1i91**	1.15(256)	-10.25	2.87
36	**3dd0**	1.00 (195)	-8.85	1.1
37	**1g53**	0.91(255)	-9.73	3.62
38	**1bnw**	0.83(254)	-10.15	3.07
39	**2f14**	0.64(257)	-10.34	3.48
40	**1bn4**	0.49(254)	-9.79	2.74
41	**1bn1**	0.46(254)	-9.88	2.14
42	**1cil**	0.37(253)	-10.02	1.25
43	**1g1d**	0.36(255)	-9.73	3.67
44	**1bnq**	0.32(254)	-9.8	1.25
45	**1g52**	0.29(255)	-9.36	1.05
46	**1if8**	0.23(258)	-10.46	1.94
47	**1bnu**	0.20 (254)	-10.08	1.14
48	**1bnt**	0.16(254)	-10.58	1.51
49	**1bn3**	0.13(254)	-10.34	0.62
50	**1bnn**	0.12(254)	-10.24	0.48
51	**1bnm**	0.10 (254)	-10.35	0.87
52	**1if7**	0.03(258)	-10.71	2.64

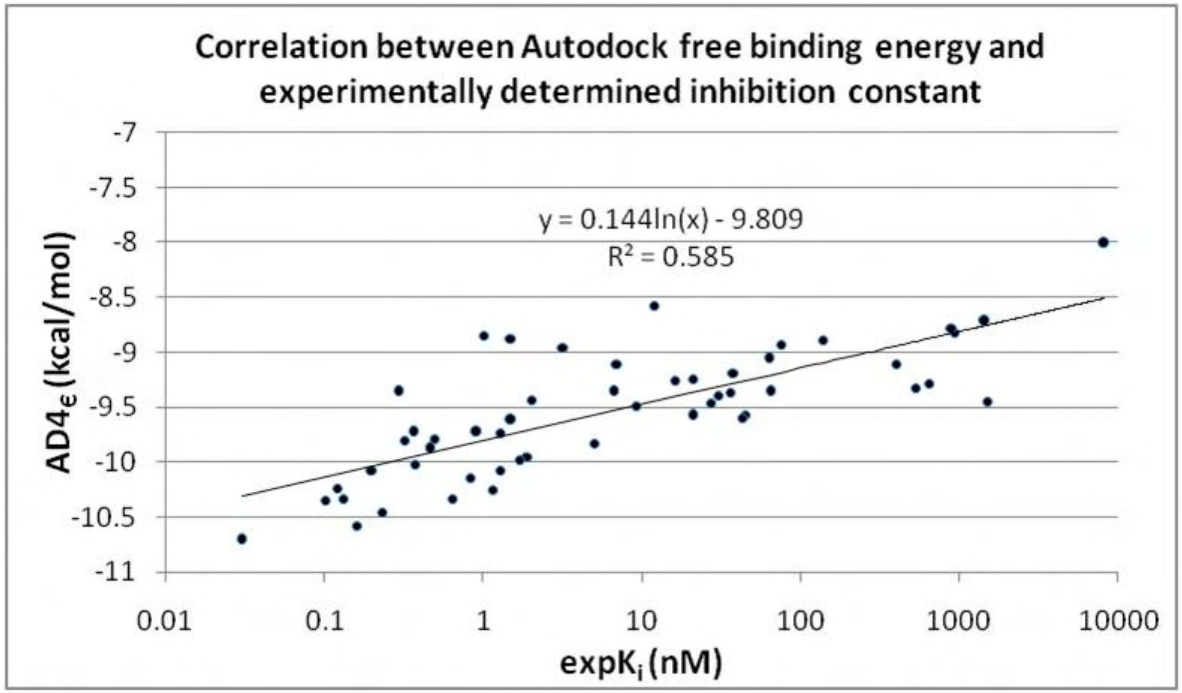

Figure 3.1: Correlation between Autodock free binding energy ($AD4_{\epsilon}$) and experimentally determined inhibition constant ($expK_i$) for carbonic anhydrase II.A coefficient of determination (R^2) of 0.5856 between $expK_i$ and $AD4_{\epsilon}$ was observed for docked ligands with known structures and $expK_i$.

Docking library of leads into CAII and a CAIX mimic

In order to generate a library of modified estradiol ligandswith potential antimitotic and anti-carbonic anhydrase activity, several modifications were made at positions 2 and the D-ring in (Table 3.2). Position 3 was replaced with a sulphamate group in all the ligands as it is known that the sulfonamido nitrogen facilitates binding to the zinc ion present in carbonic anhydrases binds (259). Modifications at position 2 were made to include moieties that are known to improve the antimitotic activity of estradiol analogs (Table 3.2). Cushman *et al.* (1995) demonstrated that 2-((*E*)-1'-propenyl and 2-ethoxy and substitutions improved the antimitotic activity of estradiol on several cancer cell lines (260). Leese *et al.* (2004) demonstrated that a 2-methylsulphanyl substitution of estradiol greatly enhanced anti-proliferative activity while the 2-ethyl substitution enhanced anti-mitotic activity even more (261, 262). Therefore, 2-methoxy, 2-ethoxy, 2-ethyl, 2-methylsulphanyl and 2-((*E*)-1'-propenyl derivatives were included in the lead library. D-ring modifications that are known to improve the anti-proliferative activity of estradiol analogues were also included (Table 3.2). These include the 17-1'-methylene substitution discovered by Edsall *et al.* (2004) (263). Dehydration at positions 14 and 15 was shown to have increased anti-proliferative and anti-tumour activities(165). The 16-dehydrated anti-mitotic analogue of 2ME (ENMD-1198) also shows promise and is currently undergoing clinical trials, therefore dehydration at position together with double dehydration at position 14 and 16 were included in the library of lead ligands (264). 17-*O*-sulphamate as well as 17-deoxy-17-cyano substitutions have also shown promise and were thus included in the docking study (265, 266) (Table 3.2). 17-hydroxy as well as 17-keto substitutions were also considered. All the modifications were made to generate a library of leads containing 85 ligands (Table 3.2).

After docking the library of estrone analog ligands into the active sites of CAII and the CAIX mimic, it was observed that the3-methoxy, 2-ethyl and 2-methylsulphanyl moieties performed better than the other sterically largermoieties in both isoforms of CAs (Table 3.3). The approximate $expK_i$ of the best $AD4_C$ score of each ligand was calculatedusing the following formula that was derived from the logarithmicfunction in Figure 3.1 (Table 3.4).

$$expK_i = e^{\frac{AD4_C + 9.809}{0.144}}$$

The CAIX mimic:CAII ratio was calculated and ratios that are less than 1 indicate that the leads are possibly more selective towards CAIX than to CAII (Table 3.4). Twelve estradiol derivatives, compounds number 14, 16, 4, 48, 50, 35, 6, 1, 2, 31, 37 and 15 in descending order, has ratio of less than 1 (Table 3.5). Six out of these twelve leads were dehydrated at position 15. Four out of the twelve leads were 2-ethyl derivatives and seven out of the twelve were 2-hydroxy derivatives.

The crystal structure of derivatives Test 6 bound to CAII has been resolved prior to the synthesis of the novel compounds in the present study. Derivative six is the 2-methoxy-3-O-sulfamoyl-17β-cyanomethyl estra-1,3,5(10)-triene estradiol analogue and is bound to CAII in the 3BET Protein Data Bank file (237). The RMSD for derivative six of the docked position compared to the crystal structure is 1.02Å, indicating that the docking software can reproduce the correct docking pose for this particular estradiol analogue (Table 3.1). After the synthesis of the novel compounds in this study, several groups resolved the crystal structures of other estradiol analogues bound to CAII as well as the CAIX mimic.

Leese *et al.* (2010) resolved the structure of derivative Test 2 (2-methoxyestradiol-bis-sulfamate, 2gd8)bound to CAII (262). Cozier *et al.* (2010) resolved the structure of derivative Test 36 bound to CAII (2-ethoxyestradiol-bis-sulfamate, 2x7t) while Sippel *et al.* (2011) resolved the structure of derivative Test 36 bound to the CAIX mimic (3oik) (194, 267). Sippel *et al.* (2011) also resolved the structures for derivatives Test 37 (3oku for CAII and 3okv for the CAIX mimic) and Test 38 (3oim for CAII and 3oil for the CAIX mimic)(194). The RMSD of the docking poses for derivatives Test 2, Test 36, Test 37 and Test 38 for CAII as well as the CAIX mimic were all less than Test 2, further indicating that the correct docking poses for estradiol derivatives into CAII and the CAIX mimic are correctly predicted with Autodock (Table 3.6).

Table 3.2: Structures of estradiol ligands generated by modifying various constituents at position 2' and the D-ring of estrone.Test 1-17 are 3-sulphamoyl-estrone analogs with a 2-methoxy group (group 1), Test 18-34 are 3-sulphamoyl-estrone analogs with a 2-ethoxy group (group 2), Test 35-51 are 3-sulphamoyl-estrone analogs with a 2-ethyl group (group 3), Test 52-68 are 3-sulphamoyl-estrone analogs with a 2-methylsulphanyl group (group 4) and Test 69-85 are estradiol compounds with a 2-((*E*)-1'-propenyl group (group 5). D-ring modifications include dehydration at position 14 (Test 7-12, 24-29, 42-47, 59-64, 75-80) (group II A-F), position 15 (Test 13-17, 30-34, 49-52, 65-69, 81-85) (group III B-F) and position 16 (Test 1, 7, 18, 24, 35, 42, 52, 59, 69 amd 75) (group 1-A). Group B (Test 2, 8, 14, 19, 25, 31, 37, 43, 49, 54, 60, 66, 70, 76 and 81) contain the 17-*O*-sulphamate modification. Group C (Test 3, 9, 15, 20, 26, 32, 38, 44, 50, 55, 61, 67, 71, 77 and 82) contain the 17-*O*-sulphamate modification.17-keto modification. Group D (Test 4, 10, 16, 21, 27, 33, 39, 45, 51, 56, 62, 68, 72, 78 and 83) contain the 17-hydroxyl modification. Group E (Test 5, 11, 17, 22, 28, 34, 40, 46, 52, 57, 63, 69, 73, 79 and 84) contain the 17-1'-methylene modification. Group F (Test 6, 12, 18, 23, 29, 35, 41, 47, 53, 58, 64, 70, 74, 80 and 85) contain the 17-cyano modification.

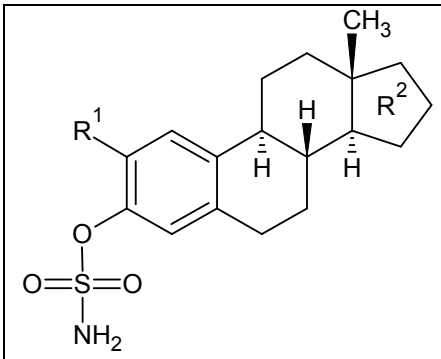		**1**	**2**	**3**	**4**	**5**
		R^1				
		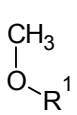	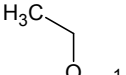			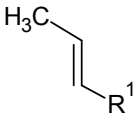
	R^2					
I-A	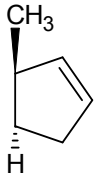	**Test 1**	**Test 18**	**Test 35**	**Test 52**	**Test 69**
I-B	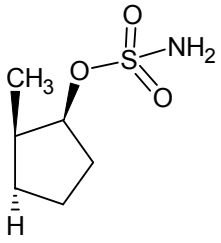	**Test 2**	**Test 19**	**Test 36**	**Test 53**	**Test 70**

I-C	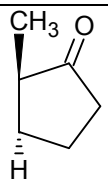	**Test 3**	**Test 20**	**Test 37**	**Test 54**	**Test 71**
I-D	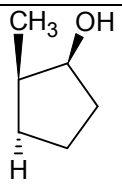	**Test 4**	**Test 21**	**Test 38**	**Test 55**	**Test 72**
I-E	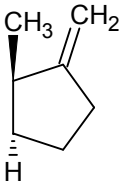	**Test 5**	**Test 22**	**Test 39**	**Test 56**	**Test 73**
I-F	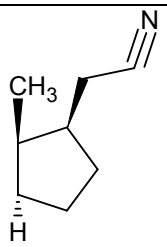	**Test 6**	**Test 23**	**Test 40**	**Test 57**	**Test 74**
II-A	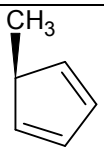	**Test 7**	**Test 24**	**Test 41**	**Test 58**	**Test 75**
II-B	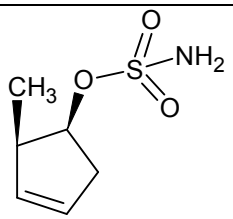	**Test 8**	**Test 25**	**Test 42**	**Test 59**	**Test 76**
II-C	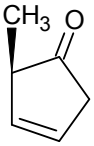	**Test 9**	**Test 26**	**Test 43**	**Test 60**	**Test 77**
II-D	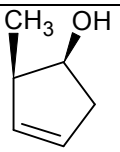	**Test 10**	**Test 27**	**Test 44**	**Test 61**	**Test 78**

II-E	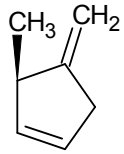	**Test 11**	**Test 28**	**Test 45**	**Test 62**	**Test 79**
II-F	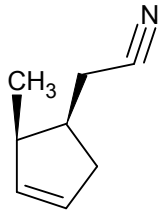	**Test 12**	**Test 29**	**Test 46**	**Test 63**	**Test 80**
III-B	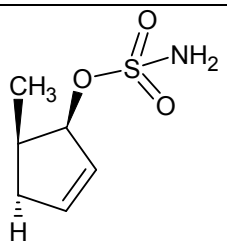	**Test 13**	**Test 30**	**Test 47**	**Test 64**	**Test 81**
III-C	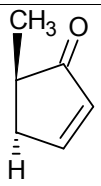	**Test 14**	**Test 31**	**Test 48**	**Test 65**	**Test 82**
III-D	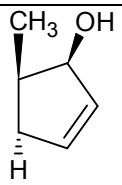	**Test 15**	**Test 32**	**Test 49**	**Test 66**	**Test 83**
III-E	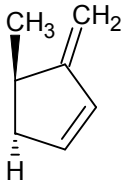	**Test 16**	**Test 33**	**Test 50**	**Test 67**	**Test 84**
III-F	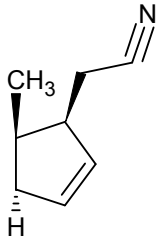	**Test 17**	**Test 34**	**Test 51**	**Test 68**	**Test 85**

Table 3.3: Best docking energy of estrone analogs docked into CAII and a CAIX mimic.Ligands where docked into 1OKN, 1KWR, 1CIM, 1BNW, 1CNX, 1OQ5 and 1TTM for X-ray structures for CAII and 3DC9, 3DCS, 3DCC, 3DC3, 3DCW and 3DBU X-ray structures for CAIX.

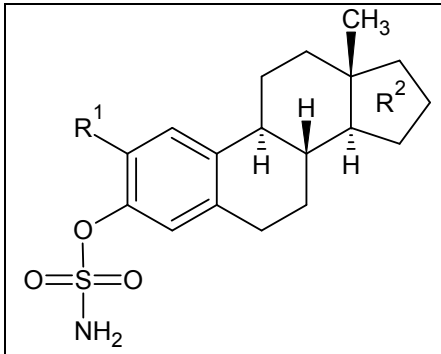		**1** 		**2** 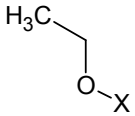		**3** 		**4** 		**5** 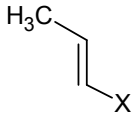	
		Autodock 4.0 docking energy after docking into the CAIX mimic and CAII									
		CAIX	**CAII**	**CAIX**	**CAII**	**CAIX**	**CAII**	**CAIX**	**CAII**	**CAIX**	**CAII**
I-A	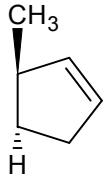	-9.86	-9.72	-9.64	-9.78	-10.06	-9.89	-9.41	-9.72	-8.41	-9.90
I-B	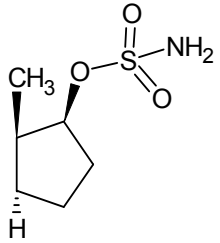	-9.13	-9.02	-9.03	-9.46	-9.14	-9.58	-9.30	-9.57	-9.43	-9.81

I-C	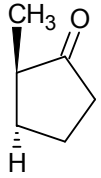	-9.70	-9.73	-9.47	-9.56	-9.90	-9.89	-9.15	-9.59	-7.96	-9.70
I-D	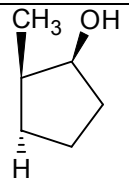	-9.46	-9.27	-8.51	-9.30	-9.32	-9.48	-9.34	-9.51	-7.69	-9.48
I-E	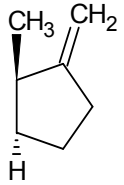	-9.66	-9.84	-9.02	-9.91	-9.78	-10.01	-9.73	-9.85	-7.94	-9.88
I-F	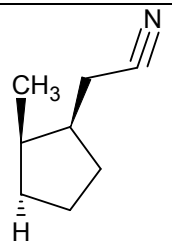	-9.04	-8.90	-8.12	-9.81	-9.07	-9.54	-8.67	-9.68	-7.90	-9.59
II-A	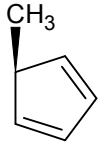	-9.49	-9.64	-9.13	-9.83	-9.80	-9.94	-9.11	-9.78	-8.14	-10.33

II-B	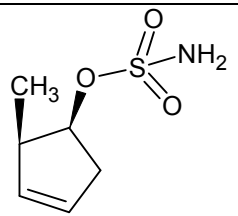	-9.46	-9.48	-9.45	-9.52	-9.44	-9.69	-9.30	-9.47	-9.78	-9.78
II-C	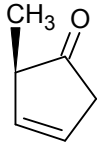	-9.50	-9.68	-8.94	-9.79	-9.77	-9.97	-9.00	-9.75	-8.14	-10.03
II-D	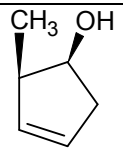	-9.32	-9.51	-8.69	-9.51	-9.45	-9.80	-8.82	-9.46	-7.83	-9.72
II-E	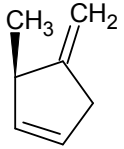	-9.82	-9.94	-8.68	-9.80	-10.07	-10.08	-9.40	-10.04	-8.40	-10.11
II-F	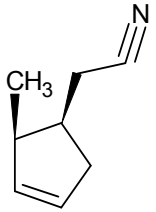	-9.70	-9.82	-8.83	-9.66	-9.55	-9.97	-9.62	-9.85	-8.11	-9.88

III-B	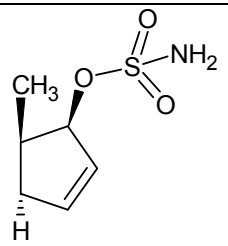	-9.23	-9.64	-9.31	-9.51	-9.28	-9.51	-9.43	-9.61	-9.22	-10.04
III-C	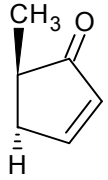	-9.77	-9.59	-9.49	-9.45	-9.88	-9.69	-8.84	-9.55	-8.26	-9.73
III-D	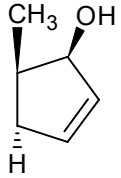	-9.20	-9.27	-8.54	-9.38	-9.24	-9.45	-8.10	-9.21	-7.73	-9.53
III-E	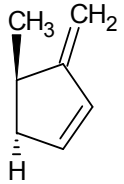	-9.90	-9.74	-9.00	-9.70	-9.96	-9.79	-9.52	-9.80	-8.32	-9.99
III-F	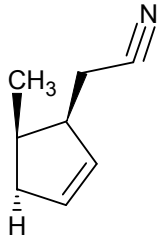	-8.98	-9.53	-8.94	-9.65	-8.88	-9.73	-8.49	-9.51	-8.14	-9.69

Table 3.4: The CAIX:CAII ratio of transformed expK_i nM values.

	CAIX (Transformed expK_i - nM)	CAII (Transformed expK_i - nM)	CAIX:CAII ratio
Test 1	0.7	1.8	0.4
Test 2	111.3	234.1	0.5
Test 3	2.1	1.7	1.3
Test 4	10.9	42.3	0.3
Test 5	2.7	0.8	3.4
Test 6	207.5	531.7	0.4
Test 7	8.7	3.2	2.7
Test 8	11.0	9.4	1.2
Test 9	8.2	2.4	3.4
Test 10	29.9	8.0	3.7
Test 11	0.9	0.4	2.3
Test 12	2.0	0.9	2.2
Test 13	54.9	3.2	17.1
Test 14	0.4	4.6	0.1
Test 15	37.3	40.7	0.9
Test 16	0.3	1.6	0.2
Test 17	663.5	7.0	94.8
Test 18	3.2	1.2	2.6
Test 19	222.3	11.3	19.8
Test 20	10.6	5.6	1.9
Test 21	7687.9	32.4	237.2
Test 22	231.8	0.5	482.5
Test 23	120780.5	1.0	119793.5
Test 24	108.2	0.9	123.3
Test 25	12.2	7.4	1.7
Test 26	392.1	1.1	355.8
Test 27	2274.3	7.7	297.2

Test 28	2437.2	1.0	2323.6
Test 29	875.1	2.8	310.4
Test 30	31.1	7.7	4.1
Test 31	9.2	11.8	0.8
Test 32	6333.7	19.4	326.8
Test 33	273.6	2.1	133.2
Test 34	397.6	3.0	131.6
Test 35	0.2	0.6	0.3
Test 36	99.6	4.7	21.3
Test 37	0.5	0.6	0.9
Test 38	28.7	9.3	3.1
Test 39	1.2	0.3	4.9
Test 40	168.6	6.2	27.1
Test 41	1.1	0.4	2.7
Test 42	12.8	2.3	5.7
Test 43	1.3	0.3	4.0
Test 44	12.2	1.0	11.9
Test 45	0.2	0.2	1.0
Test 46	0.4	0.3	1.4
Test 47	37.3	7.6	4.9
Test 48	0.6	2.3	0.3
Test 49	51.3	11.8	4.3
Test 50	0.3	1.1	0.3
Test 51	602.3	1.8	343.4
Test 52	15.8	1.8	8.8
Test 53	33.8	5.1	6.7
Test 54	91.7	4.4	20.6
Test 55	25.7	7.8	3.3
Test 56	1.7	0.7	2.3
Test 57	2685.2	2.4	1115.8
Test 58	127.8	1.2	109.3

Test 59	32.9	10.6	3.1
Test 60	258.9	1.5	178.1
Test 61	925.0	11.4	81.4
Test 62	16.9	0.2	82.5
Test 63	3.7	0.7	5.1
Test 64	13.8	3.8	3.6
Test 65	828.0	5.8	142.7
Test 66	131239.0	61.6	2130.0
Test 67	7.2	1.1	6.8
Test 68	9331.7	7.9	1184.0
Test 69	15789.9	0.5	30074.1
Test 70	13.6	1.0	13.7
Test 71	365490.9	2.0	179667.5
Test 72	2367887.2	9.4	251449.5
Test 73	402673.9	0.6	674448.8
Test 74	523796.3	4.6	114467.6
Test 75	99504.5	0.0	3827363.0
Test 76	1.2	1.2	1.0
Test 77	103723.2	0.2	490564.4
Test 78	874116.4	1.8	474348.9
Test 79	16459.4	0.1	135417.1
Test 80	129435.0	0.6	221123.3
Test 81	6.8	0.2	34.8
Test 82	43369.4	1.7	25980.5
Test 83	1795316.8	7.0	256470.8
Test 84	29031.1	0.3	106182.2
Test 85	105168.8	2.2	47297.4

Table 3.5: The compounds with the best CAIX:CAII ratios from transformed expK_i nM values after docking.

Lead		CAIX:CAII Ratio
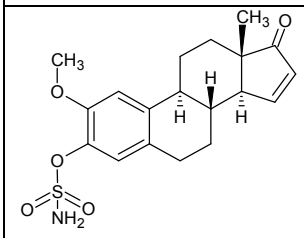	**Test 14**	0.082635
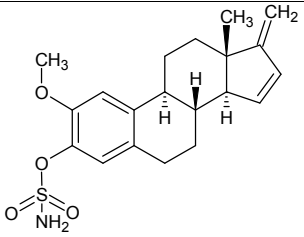	**Test 16**	0.174829
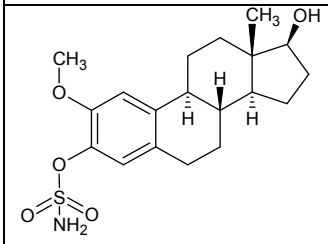	**Test 4**	0.257077
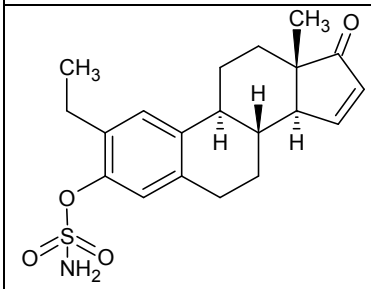	**Test 48**	0.265865
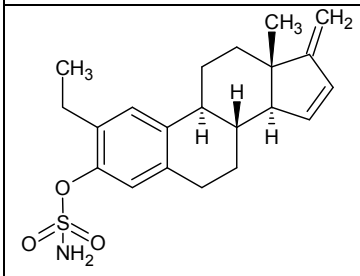	**Test 50**	0.304127

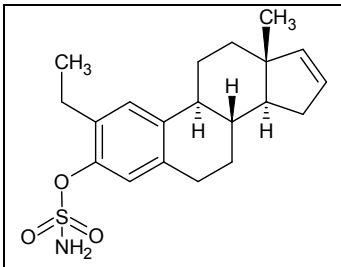	**Test 35**	0.310814
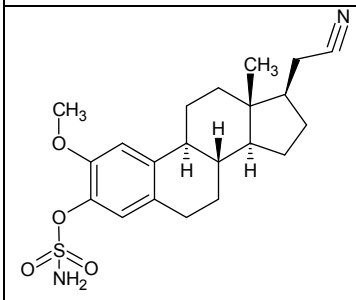	**Test 6**	0.390169
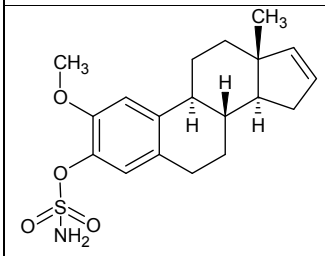	**Test 1**	0.396389
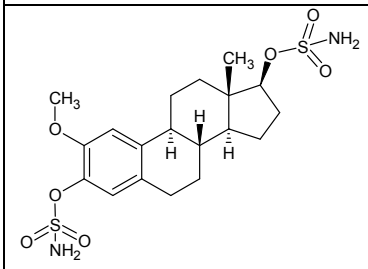	**Test 2**	0.475471
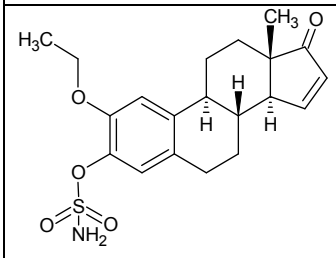	**Test 31**	0.779475

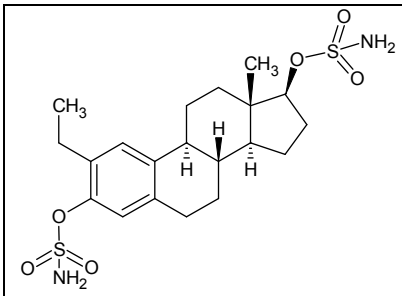	**Test 37**	0.902292
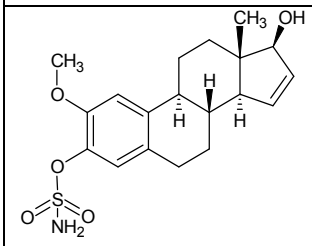	**Test 15**	0.916678

Table 3.6: The docking poses and root means squared deviation values of redocked CAII and CAIX mimic ligands. Ligands from 2gd8, 2x7t, 30ku, 3oim, 3oik, 3okv and 3oil(white) were redocked (pink) into their corresponding proteins using Autodock.

Depiction	Protein - ligand	RMSD(Å)
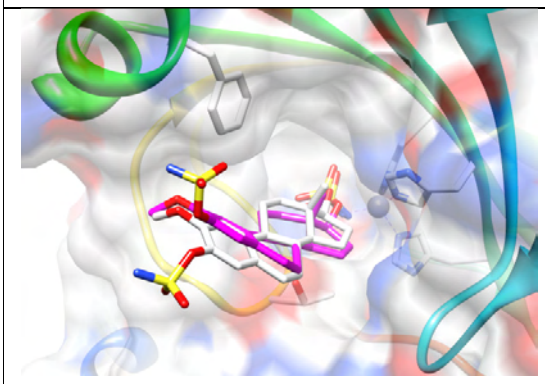	2gd8 - Test 2 (CAII)	0.77
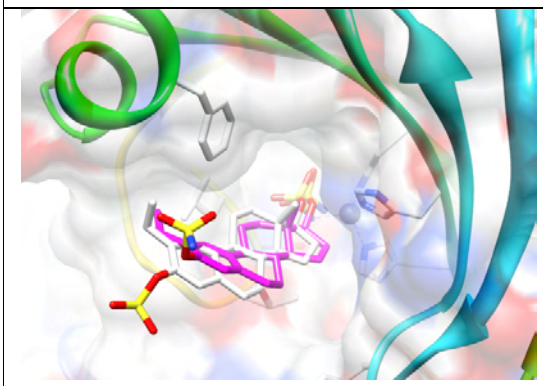	2x7t - Test 37 (CAII)	1.27
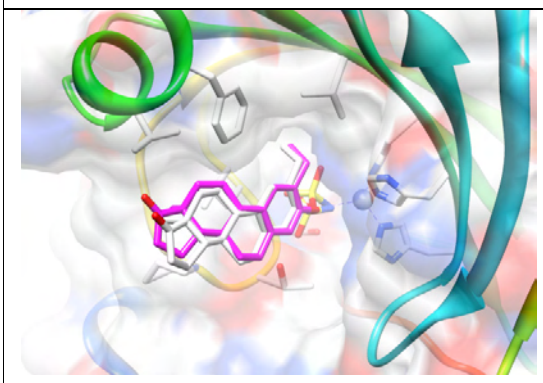	3oku - Test 38 (CAII)	1.12

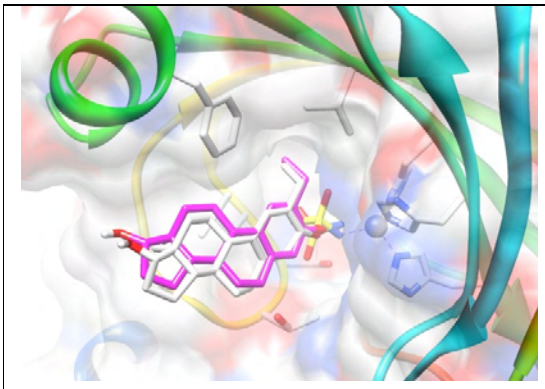	3oim - Test 39 (CAII)	0.89
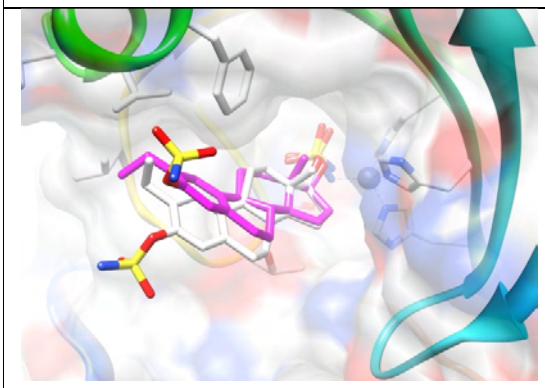	3oik - Test 37 (CAIX mimic)	1.74
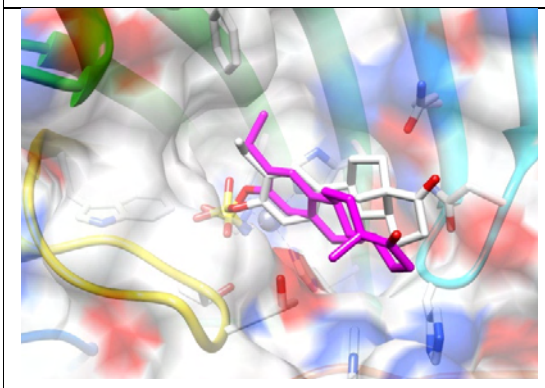	3okv - Test 38 (CAIX mimic)	1.46
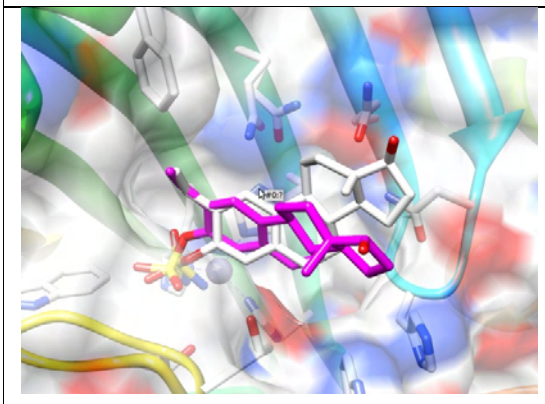	2oil - Test 39 (CAIX mimic)	1.94

Docking library of leads into Tubulin

Five crystal structures of the alpha- and beta-dimers of tubulin have been resolved and three different compounds are captured in the colchicine-binding site of tubulin. These include colchicine (2-mercapto-*n*-[1,2,3,10-tetramethoxy-9-oxo-5,6,7,9-tetrahydro-benzo[α]heptalen-7-yl]acetamide or CN2) in the 1sa0, 3du7 and 1z2b structure, another colchicine analogue *N*-[(7*S*)-1,2,3,10-tetramethoxy-9-oxo-6,7-dihydro- 5H-benzo[d]heptalen-7-yl]ethanamide (LOC) in the 2e22 structure and podophyllotoxin (9-hydroxy-5-(3,4,5-trimethoxyphenyl)-5,8,8a,9-tetrahydrofuro[3',4':6,7] naphtha [2,3-d][1,3]dioxol- 6(5ah)-one or POD) in the 1sa1 structure.

CN2, LOC and POD were redocked into their corresponding structures in order to evaluate the ability of Autodock to predict the correct pose. CN2, LOC and POD had an RMSD value of 1.21Å, 0.42Å and 0.77Å respectively (Table 3.8). All of the redocked poses had an RMSD value of less than 2, indicating that the software was able to reproduce the original crystal structure pose with reasonable accuracy.

After docking the library of estradiol derivatives into the colchicine binding site between the alpha- and beta-dimers of the tubulin protein, it was revealed that the 2-ethyl derivatives performed better than all the other derivatives when compared to their corresponding D-ring modified analogs (Table 3.7). This is in agreement with the results of Leese *et al.* (2006) where it was discovered that an ethyl substitution at position 2' of estrone provided the optimal substituent for high antiproliferative activity(262). Based on the docking results of the analogs into the colchicine site and the CAIX:CAII ratio of the compounds in Table 3.5, it was decided to synthesize the novel derivatives 35, 48 and 50. Docking of compounds 35, 48 and 50 into the colchicine binding site of tubulin all showed a similar binding pose (Figure 3.2 A). Hydrophobic interactions between the derivatives and ala250.B,leu242.B, leu248.B, leu252.B, leu255.B, lys352.B, and val318.B appear to be important (Figure 3.2 B). Also, possiblehydrogen bonds may also form between the sulfonamido nitrogenof the compounds and tyr202.B or the val238.B oxygen (Figure 3.2 B).

The compounds are derivatives of estrone and one concern is that these compounds might display estrogenic effects by binding to estrogen receptors and display agonist or antagonist activity. Cushman *et al.* (1995) synthesized several estradiol analogs and it was discovered that modifications at C-2, including 2-methoxy, 2-ethoxy, 2-1-(*E*)-propenyl, 2-ethylthio, and 2-ethylamino, decreased the estrogenicity of the compounds (260). Purohit *et al.* (1998) discovered that propyl and allyl groups at C-2 together with the sulfamate group greatly decrease the estrogenicity of the compounds to the levels comparable to propylene glycol (the vehicle control) (268). The reason for this was ascribed to the bulking of the C-2 position of the estrones (268, 269). Also, Elger *et al.* (2001) described how sulfamate substitution at C-3 leads to reduced estrogenic activity when compared to the parent steroids (270). Thus, the ethyl group at C-2 together with the sulfamate group at C-3 of the newly synthesized analogs makes it unlikely that the compounds will have any estrogenic effects.

Table 3.7: Best docked energy (kcal/mol) of estrone analogs docked into the colchicine binding.The compounds where docked into the colchicines binding site of 1sa0, 1sa1, 1z2b, 3du7, and 3e22 X-ray structures.

			1	**2**	**3**	**4**	**5**
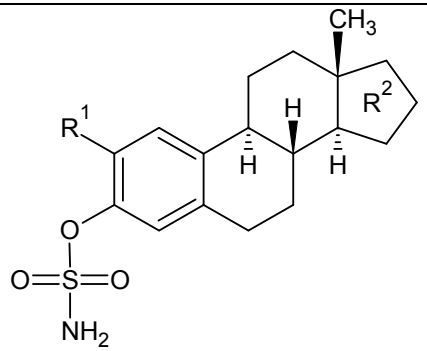			R^1				
				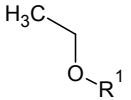			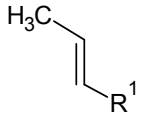
	R^2	**Rank**	**2**	**5**	**1**	**4**	**3**
I-A	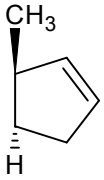	**13**	-10.05	-9.79	-10.06	-9.75	-9.48
I-B	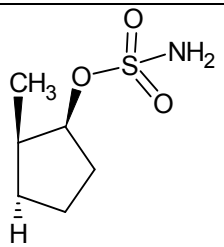	**2**	-11.04	-11.02	-11.05	-10.85	-10.99
I-C	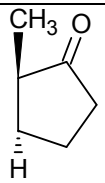	**11**	-10.21	-9.69	-10.31	-10.05	-9.9

I-D		**17**	-10.02	-9.38	-10.04	-9.5	-9.75
I-E	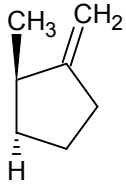	**9**	-10.39	-9.94	-10.19	-10.12	-10.06
I-F	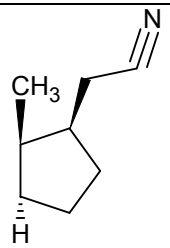	**3**	-11.34	-10.58	-11.53	-10.32	-11.01
II-A	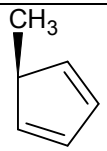	**14**	-9.58	-9.71	-9.96	-10.06	-9.96
II-B	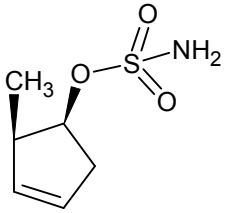	**1**	-10.83	-11.1	-11.43	-11.03	-11.27

II-C	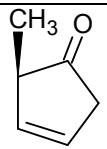	**12**	-9.71	-9.75	-10.24	-9.99	-10.32
II-D	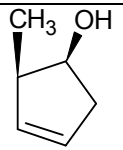	**15**	-9.73	-10.02	-9.98	-9.67	-9.74
II-E	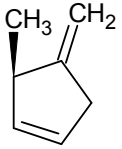	**7**	-10.2	-10.13	-10.57	-10.66	-10.61
II-F	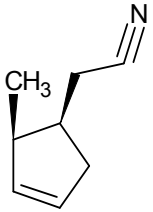	**6**	-10.68	-10.43	-11.22	-10.51	-10.88
III-B	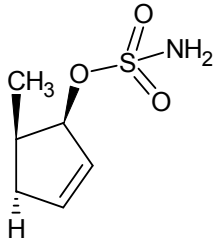	**4**	-10.8	-10.73	-10.75	-10.91	-11.06

III-C	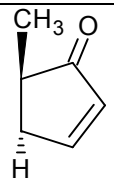	**10**	-10.19	-10.18	-10.28	-9.99	-10.04
III-D	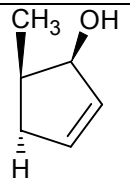	**16**	-9.88	-9.58	-10.04	-9.76	-9.79
III-E	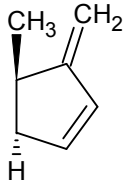	**8**	-10.24	-10.33	-10.34	-10.13	-9.91
III-F	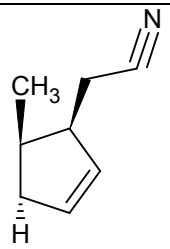	**5**	-10.95	-10.47	-11.28	-10.37	-10.62

Table 3.8: Docking poses and root means squared deviation values of ligands binding to the colchicines binding site of tubulin.Docking poses and root means squared deviation values of CN2 (2-mercapto-n-[1,2,3,10-tetramethoxy-9-oxo-5,6,7,9-tetrahydro-benzo[α]heptalen-7-yl]acetamide), LOC (N-[(7S)-1,2,3,10-tetramethoxy-9-oxo-6,7-dihydro-5H-benzo[d]heptalen-7-yl]ethanamide and POD (9-hydroxy-5-(3,4,5-trimethoxyphenyl)-5,8,8a,9-tetrahydrofuro[3',4':6,7] naphtha [2,3-d][1,3]dioxol- 6(5ah)-one) redocked into 1sa0, 2e22 and 1sa1 respectively.

	Depiction	RMSD (Å)	Receptor
CN2 **Pink: Crystal pose** **White: Redocked pose**	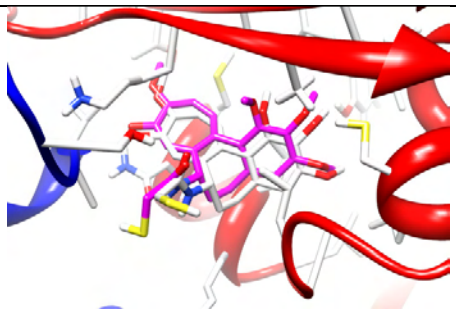	1.21	**1sa0_A**
LOC **Pink: Crystal pose** **White: Redocked pose**	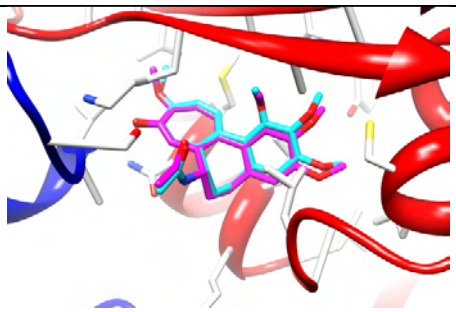	0.42	**2e22_B**
POD **Light blue: Crystal pose** **Yellow: Redocked pose**	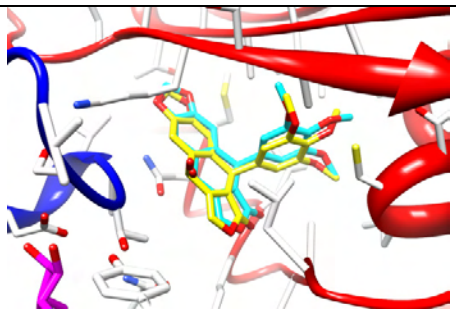	0.77	**1sa1_A**

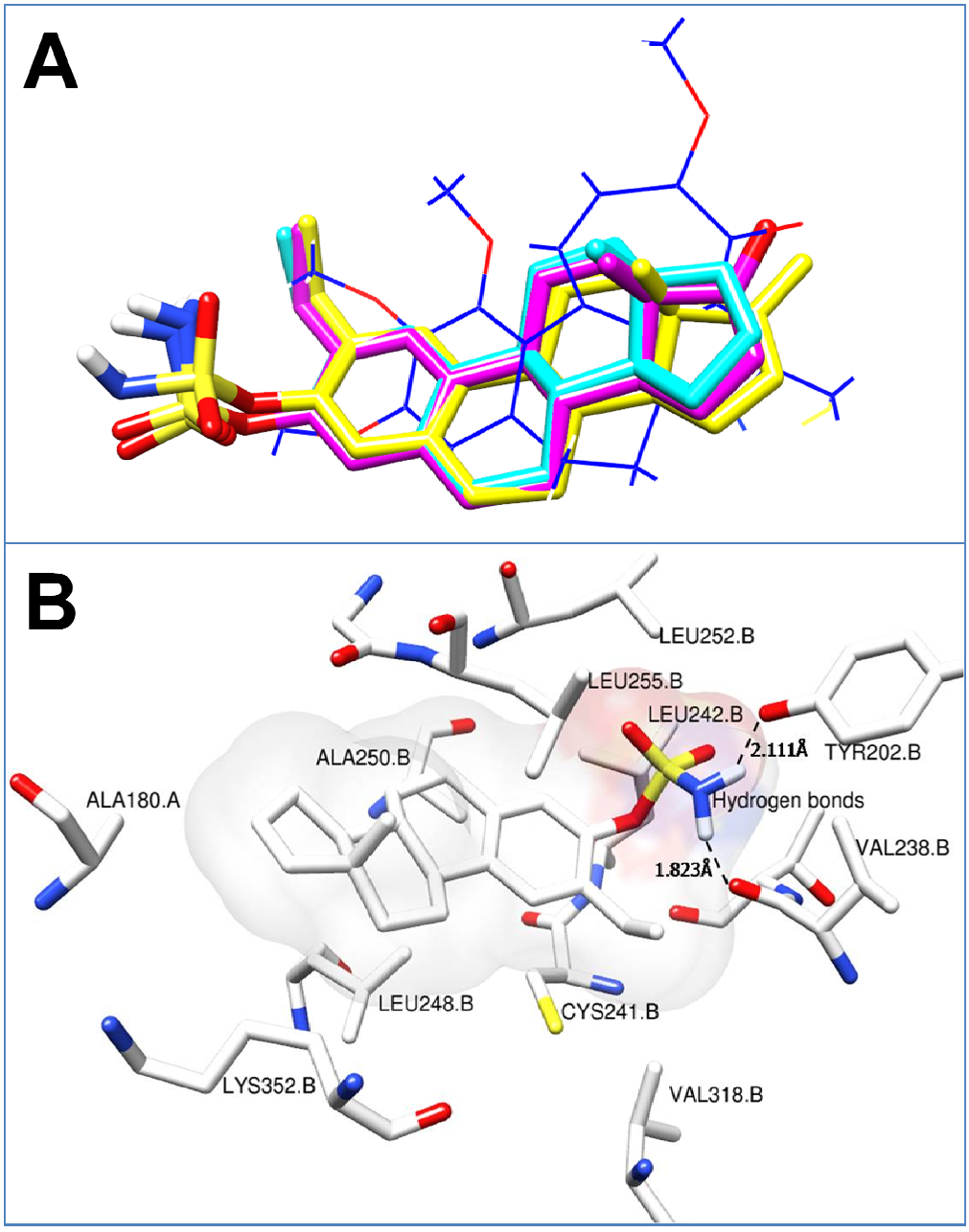

Figure 3.2: Docking of compounds 35, 48 and 50 into the colchicine binding site of tubulin. Compound35 (A, cyan), compound 48 (A, yellow) and compound 50 (A, pink) docked in the same position in the colchicines binding site as seen by the position of the crystal structure of colchicines (CN2) (A, dark blue structure). Hydrophobic interactions between compound 35 and ala250.B, leu242.B, leu248.B, leu252.B, leu255.B, lys352.B, and val318.B are observed (B). Possible hydrogen bonds may also form between the sulfonamido nitrogen of the compound and tyr202.B or the val238.B oxygen (B).

Synthesis of novel compounds

The synthesis of the lead compounds was outsourced to a private company iThembaPharmaceuticals (Pty) Ltd (Modderfontein, Gauteng, South Africa).All chemicals were purchased from Aldrich Chemical Co. (Milwaukee,WI, USA). The company is an emerging drug discovery company that is founded by researchers and eminent academics from around the world with investments from the two separate BRICs, LIFElab and BioPAD.

Derivatives Test 35, Test 48 and Test 50 are all novel 2-ethyl derivatives. The literature surrounding modifications of estrone and estradiol was investigated in order to propose a synthesis pathway for the compounds. It was discovered that the 2-ethyl estrone is a useful precursor for the synthesis of the selected precursors, as well as derivative 34 (Figure 3.3).The reason for adding derivative Test 33 is that the 17-1'-methylene substitution is easily accessible from estrone andthis particular substitution performed relatively well in the docking into tubulin compared to others (Table 3.7). Leese *et al.* (2005) have previously described the synthesis of 2-ethyl estrone from estrone (Figure 3.3, compound 1-5), therefore an initial proposal for the cost effective synthesis of 2-ethyl estrone from estrone allowed iThembaPharmaceuticals to synthesize the selected derivatives from this precursor (271).

Edsall *et al.* (2004) have previously described the synthesis of the 17-1'-methylene substitution from the carbonyl at position 17 (Figure 3.3, compound 6 from compound 5 and compound 15 from compound 13)(263). Rao *et al.* (2008) have described the synthesis of 16-dehydrated analogs (Figure 3.3, compounds 8 to 9 from compound 4) (272). Rao *et al.* (2002) described the synthesis of 15 dehydrated analogues with compound 4 in Figure 3.3 as a similar starting molecule (Figure 3.3, compounds 12 and 13 from compound 11) (272). The sulfamoylation of the 2-hydroxy was carried out by the method developed by Woo *et al.* (1996) (Figure 3.3, compound 10 from compound 9, compound 7 from compound 6, compound 14 from compound 13, and compound 16 from compound 15) (273).

The initial proposal was modified and improved by Dr Garreth Morgans (PhD in Chemistry, University of Witwatersrand) to yield a final agreement between the University of Pretoria and iThembaPharmaceuticals (Pty) Ltd for the synthesis of the compounds (Figure 3.4). It was decided not to synthesize derivative Test 50 as it may turn out to be an unstable compound with a short half-life due the two closely associated reactive carbon double bonds at positions 15 and 17. Furthermore, it was decided that derivatives Test 36 (compound 15 in Figure 3.4), Test 37 (compound 13 in Figure 3.4) and Test 38 (compound 14 in Figure 3.4) should be added as they are easily accessible from 2 ethyl estron. Also, Leese *et al.* (2005) have demonstrated that these compounds are able to induce growth inhibition in cancer cells in nanomolar concentration, thereby ensuring that we will have at least three biologically active compounds from the project (271). After initial attempts and failure to synthesize the 17-1'-methylene substitution from the carbonyl at position 17 (compound 6 in Figure 3.3 and compound 11 in Figure 3.4) a new proposal was agreed upon. Derivative Test 47 (Test 47 in Table 3.2), derivative Test 49 (Test 49 in Table 3.2) and derivative Test 2 (test 2 in Table 3.2) were included in the synthesis scheme (Figure 3.5). However, derivative Test 47 could not be isolated as it was inherently unstable and decomposed upon isolation via column chromatography.

iThemba Pharmaceuticals purchased all chemicals from Aldrich Chemical Co. Organic solvents of analytical reagent (A.R.) grade were used. Anhydrous *N,N*-dimethylformamide and *N,N*-dimethylacetamide were purchased from Aldrich and stored under a positive pressure of N_2 after use. Tetrahydrofuran was distilled from sodium. Sulfamoyl chloride was prepared by an adaptation of the method of Appel and Berger and stored in a tightly sealed container in the fridge(274). Chromatography was performed on silica gel (70–230 mesh, Macherey Nagel). Thin layer chromatography was performed on Alugram® SIL G/UV_{254} aluminium backed plates (Macherey Nagel). Products were visualized with basic potassium permanganate solution. ^1H NMR spectra were recorded in deuterated chloroform solution (unless otherwise indicated) with a Varian 400 NMR spectrometer at 400 MHz.The compounds weresuggested to be stored in the freezer prior to use as sulfamated estrones are unstable and should be exposed to ambient temperature conditions as little as possible. The purity of all the compounds were determined at > 95%. The yield of the requested compounds (compounds 9, 10, 14, 15, 16 and 19 in Figure 3.5 is greater than 30 mg.

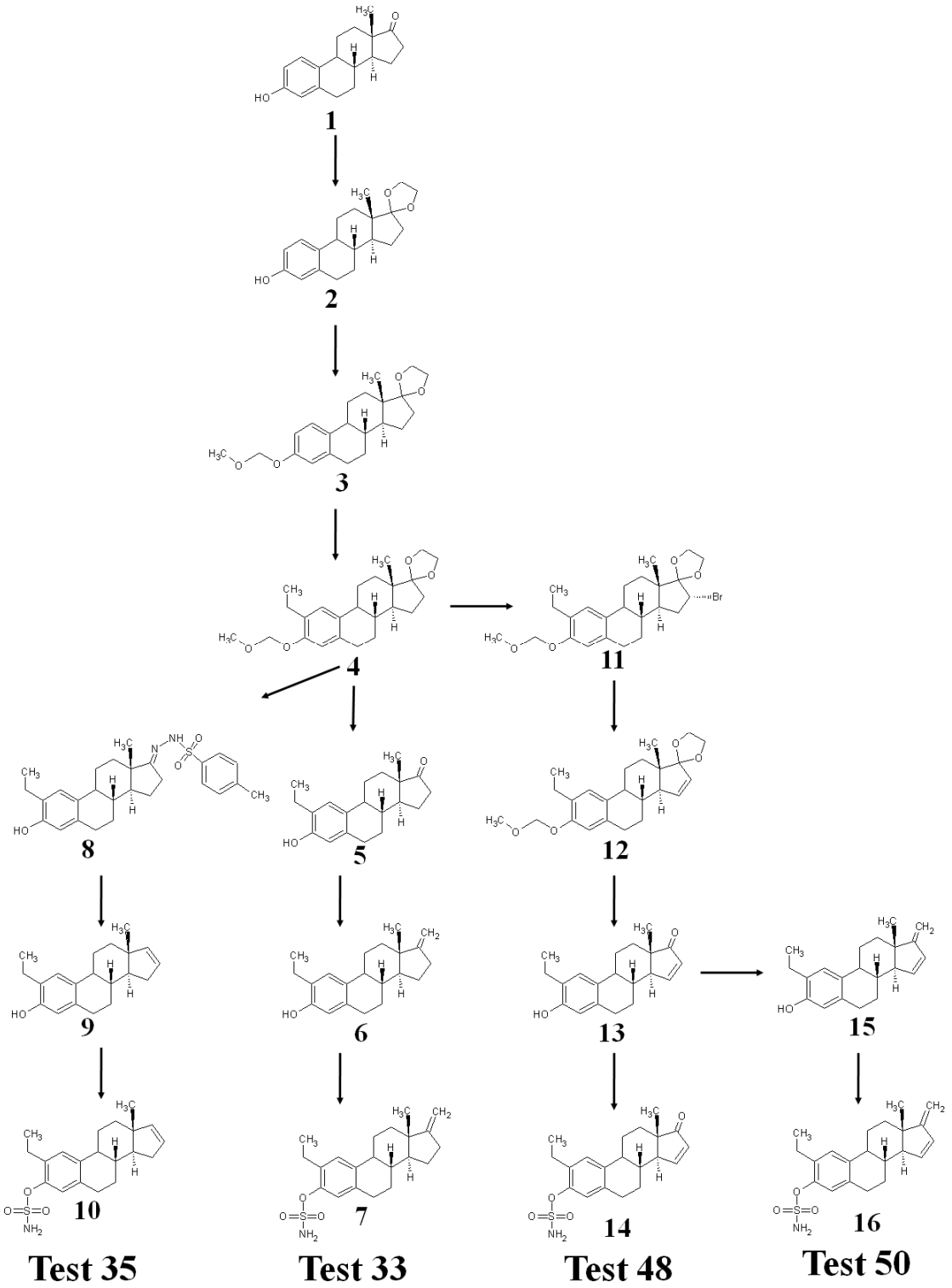

Figure 3.3: First proposed synthesis pathway for the compounds 34, 35, 48 and 50.

Project proposal from iThemba Pharmaceuticals for University of Pretoria Medical School

Proposal prepared by: Dr Garreth Morgans of iThemba Pharmaceuticals.

Comments:

This is the planned synthesis for the University Of Pretoria Medical school.

The reaction sequences exclude the preparation of sulfamoyl chloride.

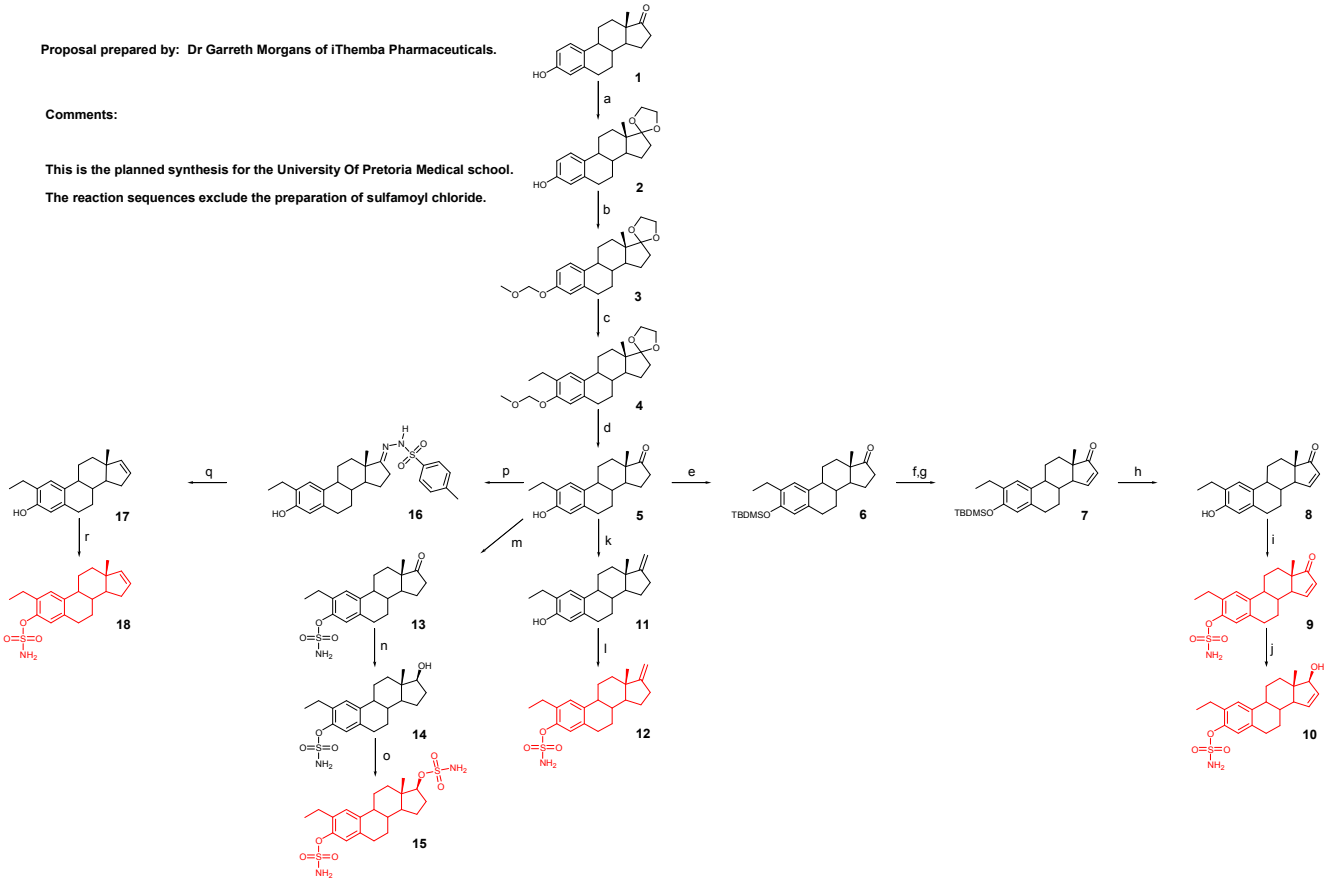

Reagents and conditions: (a) Ethylene glycol, *p*-TsOH (cat.), Dean-Stark, toluene, Δ, 16 hr; (b) NaH, MOMCl, DMF, 0 °C to rt, 16 hr; (c) *n*-BuLi, TMEDA, THF, -78 °C, 1 hr, then EtI, -78 °C to rt; (d) 6M HCl, THF, rt, 1 hr; (e) TBDMSCl, imidazole, THF, 0 °C to rt; (f) LDA, THF, -78 °C, then TMSCl; (g) $Pd(OAc)_2$, PhCN, rt, 24 h; (h) Bu_4NF, THF, rt, 2 hr; (i) Sulfamoyl chloride, DMA, 0 °C to rt, 18 hr **OR** sulfamoyl chloride, DBMP, DCM, 0 °C to rt, 16 hr; (j) $NaBH_4$, $CeCl_3.7H_2O$, MeOH, rt, 8 hr; (k) $[MeP(Ph_3)]^+Br^-$, LDA, THF, -10 °C to rt, 18 hr; (l) SAME AS (i); (m) SAME AS (i); (n) $NaBH_4$, THF/IPA, rt, 3 hr; (o) SAME AS (i); (p) *p*-Toluenesulfonylhydrazide, MeOH, Δ, 20 hr; (q) *n*-BuLi, THF, -10 °C, then rt, 3 days; (r) SAME AS (i).

Figure 3.4: Initial synthesis pathway as agreed upon between iThemba Pharmaceuticals and the Department of Physiology.

Project proposal from iThemba Pharmaceuticals for University of Pretoria Medical School

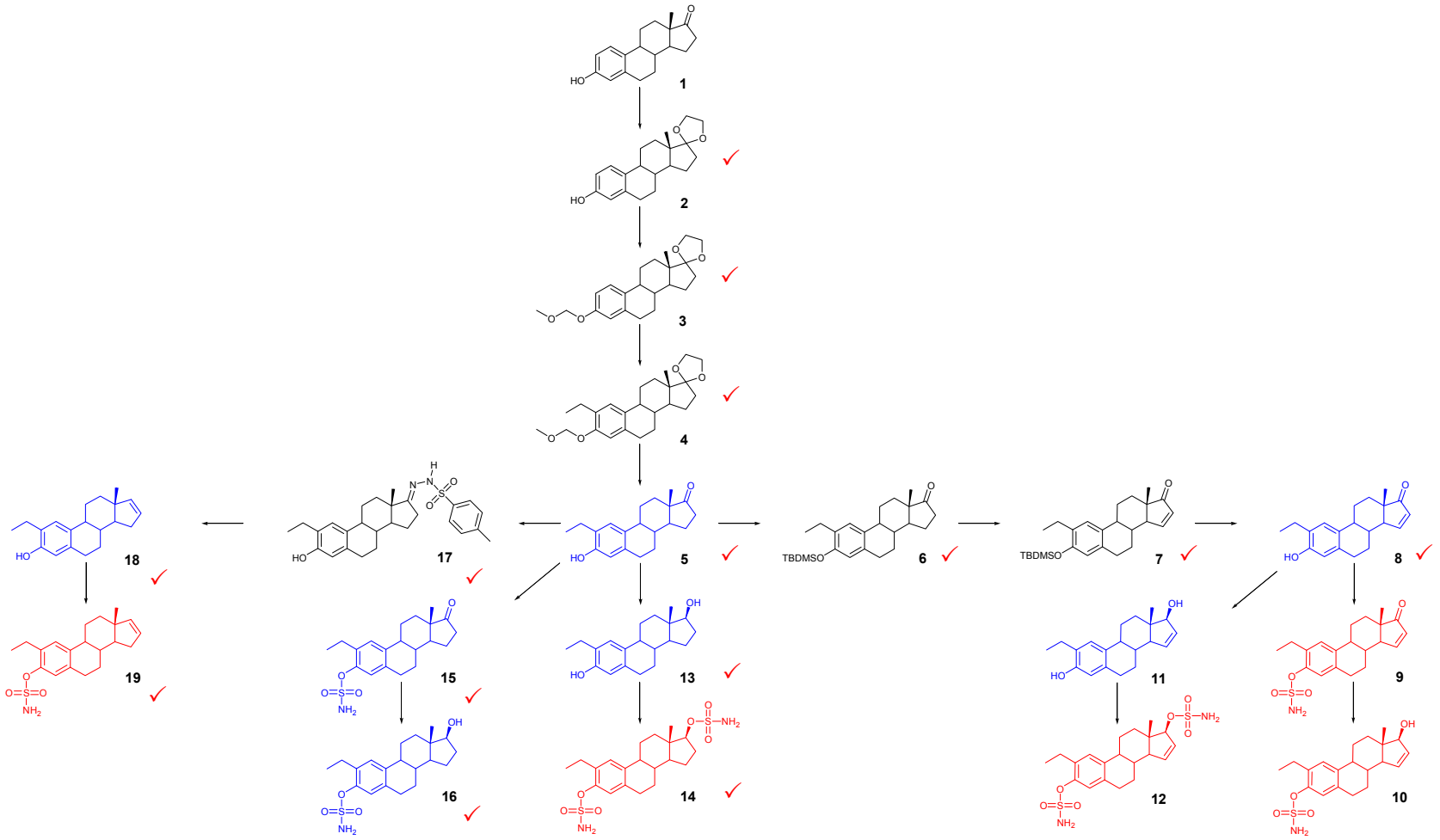

Figure 3.5: Final synthesis pathway as agreed upon between iThemba Pharmaceuticals and the Department of Physiology.This was agreed upon as a result of the failure to synthesize the 17-1'-methylene substitution from the carbonyl at position 17.

Cell growth studies

Spectrophotometry: Cell growth

Quantification of fixated monolayer cells were spectrophotometrically determined employing crystal violet as a DNA stain. Cell numbers were expressed as a percentage of the vehicle-treated control (VC). The final concentration of DMSO in the vehicle-treated control did not exceed 0.02%. After the synthesis of the novel compound 9 (2-ethyl-3-O-sulphamoyl-estra-1,3,5(10),15-tetraen-17-one, hereafter ESE-15-one), compound 10 (2-ethyl-3-O-sulphamoyl-estra-1,3,5(10),15-tetraen-17-ol, hereafter ESE-15-ol) and compound 19 (2-ethyl-3-O-sulphamoyl-estra-1,3,5(10)16-tetraene, hereafter ESE-16)(Figure 3.6), preliminary dose-dependent studies were conducted after 48 h exposure in order to determine the growth inhibitory effect of the compounds on various cell lines. A range of 50 nM to 200 nM was initially chosen in order to approximate the $GI_{50}$of each compound (Figure 3.6).

The preliminary studies indicated that ESE-15-ol was the most potent (Figure 3.6 A and Table 3.9), ESE-15-one the second most potent (Figure 3.6 B and Table 3.9) and ESE-16 the least of the three new derivatives (Figure 3.6 C and Table 3.9). Subsequent studies growth inhibitory studies over time periods of 24 h, 48 h and 72 h were performed with a narrower range of concentrations. For ESE-15-one, a range of 90 - 150 nM was chosen with intervals of 10 nM. For ESE-15-ol, a range of 30 - 50 nM was chosen with intervals of 5 nM. For ESE-16, a range of 100-220 nM with intervals of 20 nM was chosen.

The growth inhibitory effect was calculated as described by the NCI in order to compare the growth inhibition induced by the compounds on the various cell lines(275). The growth inhibitory effect was calculated by:

$$Growth\ inhibitory\ effect\ (GI) = \frac{(T - T_0)}{C - T_0} * 100$$

T is the optical density of the test well after background subtraction after 48 h exposure to test conditions.

$T_0$is the optical density after background subtraction at time of exposure (baseline).

C is the control optical density after background subtraction of the vehicle treated-control.

The 50% growth inhibitory concentration (GI_{50}) is the concentration where:

$$\frac{(T - T_0)}{C - T_0} * 100 = 50$$

Cell growth percentage over time was expressed as:

$$Cell\ growth\ \%\ over\ time = \frac{(T_x - T_0)}{T_0} * 100$$

$\mathbf{T_x}$ is the optical density of the test well after background subtraction after the amount of time of exposure for 24 h, 48 h and 72 h. T_x is equal to T_0 at the time of the exposure (0 h).

Cell growth over time using different concentrations of each compound indicated that there is a dose-dependent inhibition of cell growth with the MCF-12A cells being the least affected (Figure 3.7, Figure 3.8 and Figure 3.9). For ESE-15-one the $GI_{50}$was calculated at 130 nM, 140 nM and 150 nM for MCF-7, MDA-MB-231 and MCF-12A cells respectively (Figure 3.7 A, Figure 3.8 A, Figure 3.9 A and Figure 3.10 A).The $GI_{50}$for ESE-15-ol was calculated at 50 nM for MCF-7 and MDA-MB-231 cells and 75 nM for MCF-12A cells (Figure 3.7 B, Figure 3.8 B, Figure 3.9 B and, Figure 3.10 B). For ESE-16 the $GI_{50}$was calculated at 200 nM for MCF-7 and MDA-MB-231 and 220 nM for MCF-12A cells (Figure 3.7 C, Figure 3.8 C, Figure 3.9 C and Figure 3.10 C). Linear regression analysis was used to determine the GI_{50} of ESE-15-ol (75 nM) on MCF-12A cells (Table 3.10).

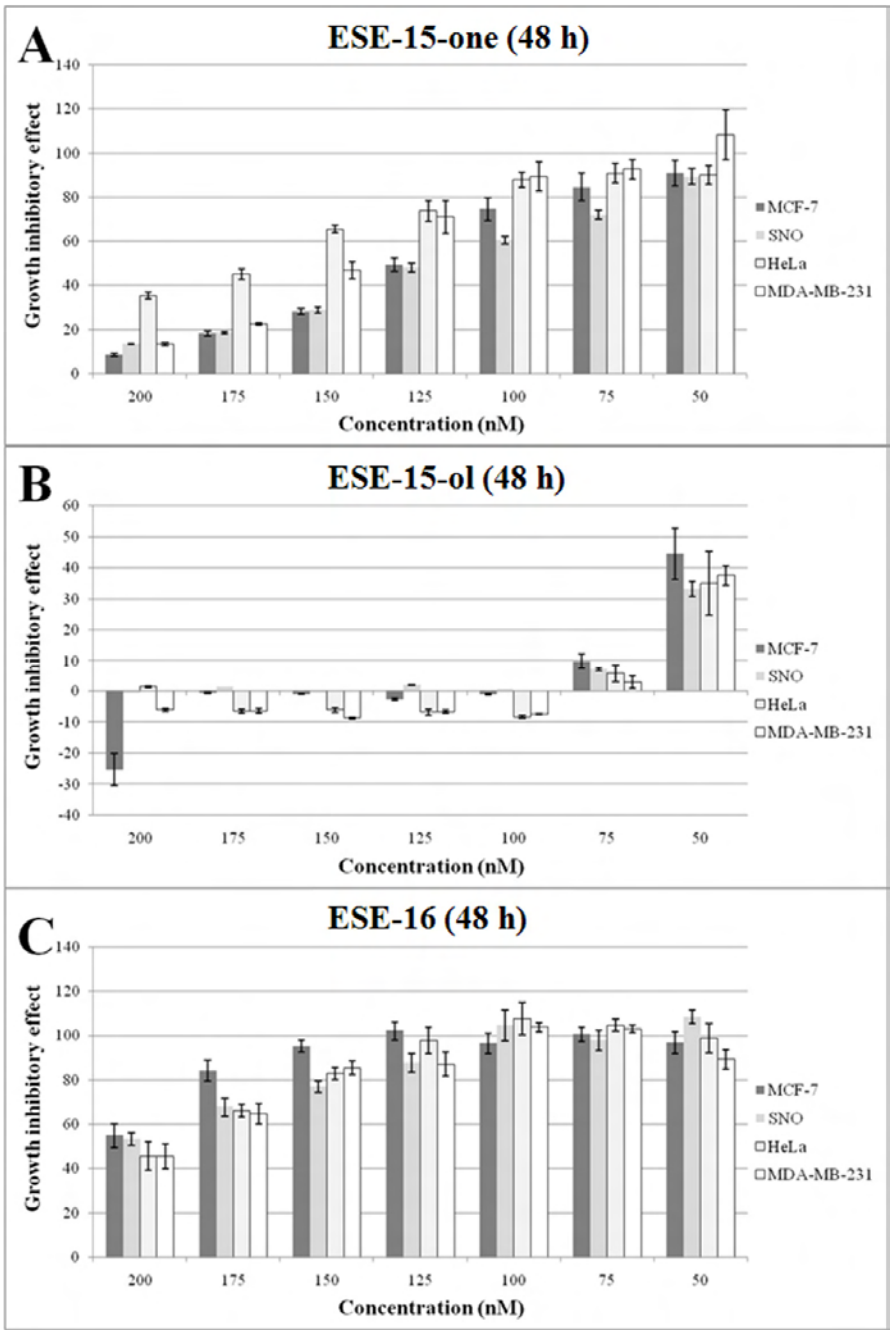

Figure 3.6: Preliminary dose-dependent studies conducted after 48 h exposure on ESE-15-one, ESE-15-ol and ESE-16. ESE-15-ol (B) was the most potent, ESE-15-one (A) the second most potent and ESE-16 (C) the least of the three new derivatives.

Table 3.9: Growth inhibitory effect of ESE-15-one, ESE-15-ol and ESE-16 after initial screening. Compounds were tested on MCF-7, SNO, MDA-MB-231 and HeLa cells. Growth inhibition = 100 x $(T-T_0)/(C-T_0)$.

Cell line	**Approximate Growth inhibitory concentration (GI_{50})**
ESE-15-one	
MCF-7	100 - 125 nM
SNO	100 - 125 nM
MDA-MB-231	150 - 175 nM
HeLa	125 - 150 nM
ESE-15-ol	
MCF-7	50 - 75 nM
SNO	50 - 75 nM
MDA-MB-231	50 - 75 nM
HeLa	50 - 75 nM
ESE-16	
MCF-7	175 - 200 nM
SNO	175 - 200 nM
MDA-MB-231	175 - 200 nM
HeLa	175 - 200 nM

Table 3.10: Growth inhibitory effect of ESE-15-one, ESE-15-ol and ESE-16 on MCF-7, MDA-MB-231 and MCF-12A cells. Growth inhibition = 100 x $(T-T_0)/(C-T_0)$.

Cell line	**Growth inhibitory concentration (GI_{50})**
ESE-15-one	
MCF-7	130 nM
MDA-MB-231	140 nM
MCF-12A	150 nM
ESE-15-ol	
MCF-7	50 nM
MDA-MB-231	50 nM
MCF-12A	75 nM
ESE-16	
MCF-7	180 nM
MDA-MB-231	200 nM
MCF-12A	220 nM

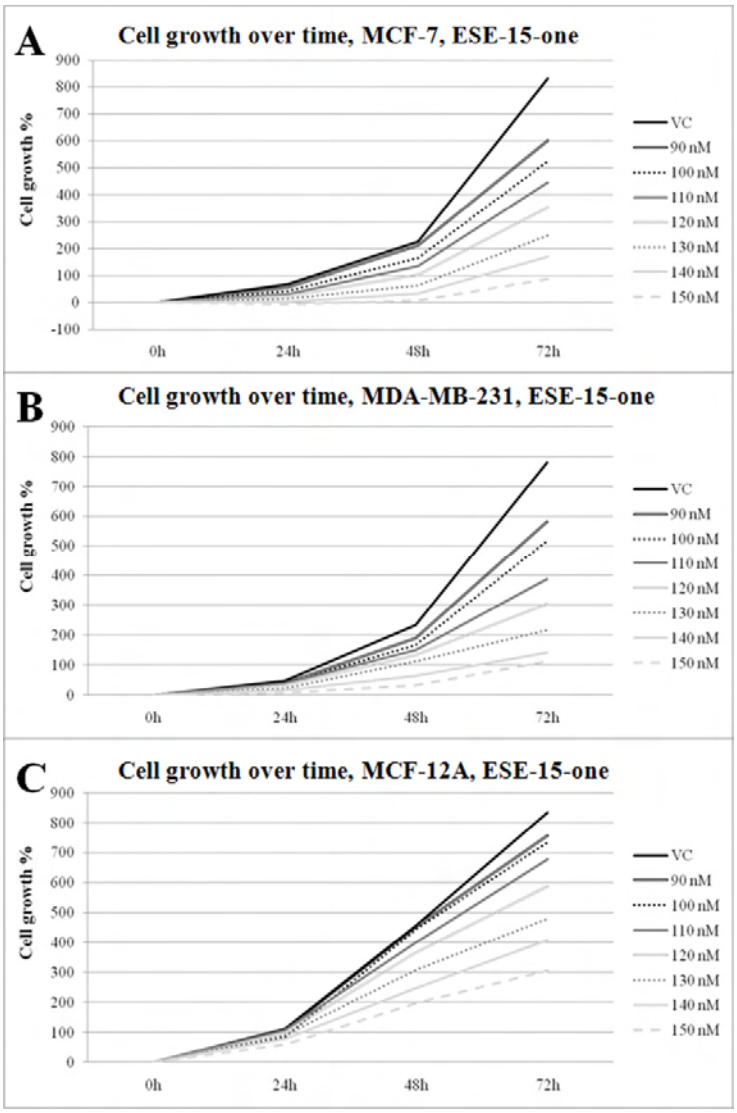

Figure 3.7: Cell growth curves over 72 h exposure for ESE-15-one on MCF-7, MDA-MB-231 and MCF-12A cells.ESE-15-one inhibited cell growth in a dose-dependent manner in the different cell lines.

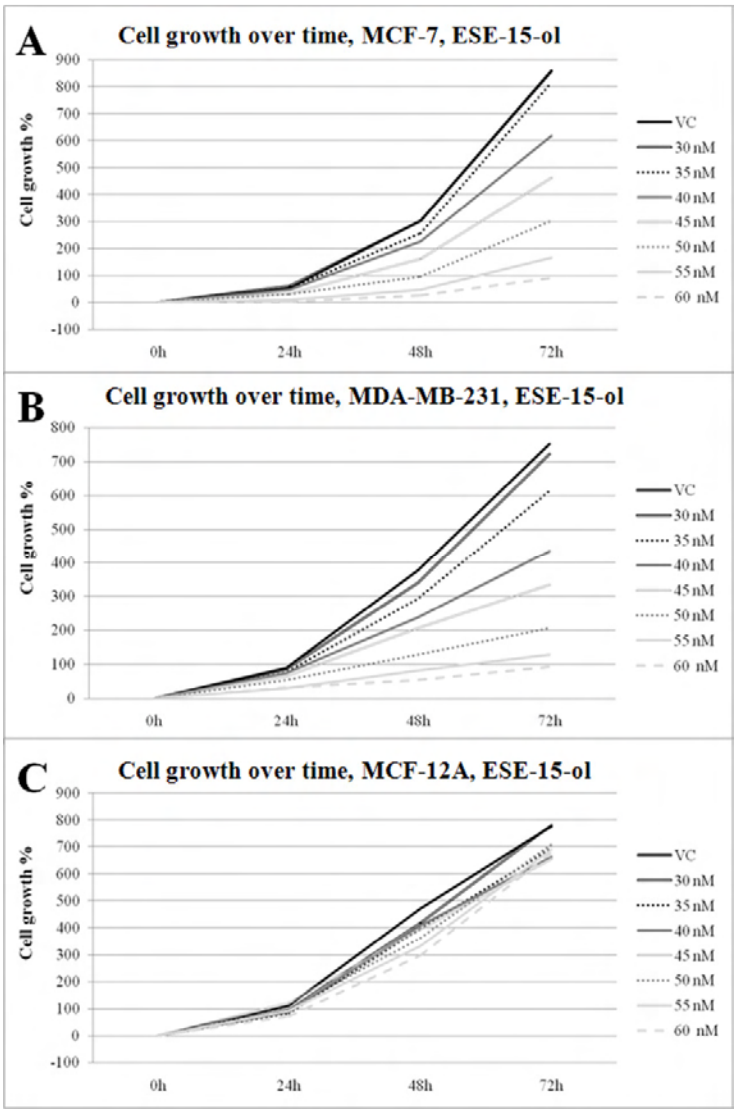

Figure 3.8: Cell growth curves over 72 h of exposure for ESE-15-ol on MCF-7, MDA-MB-231 and MCF-12A cells. ESE-15-ol inhibited cell growth in a dose-dependent manner in the different cell lines.

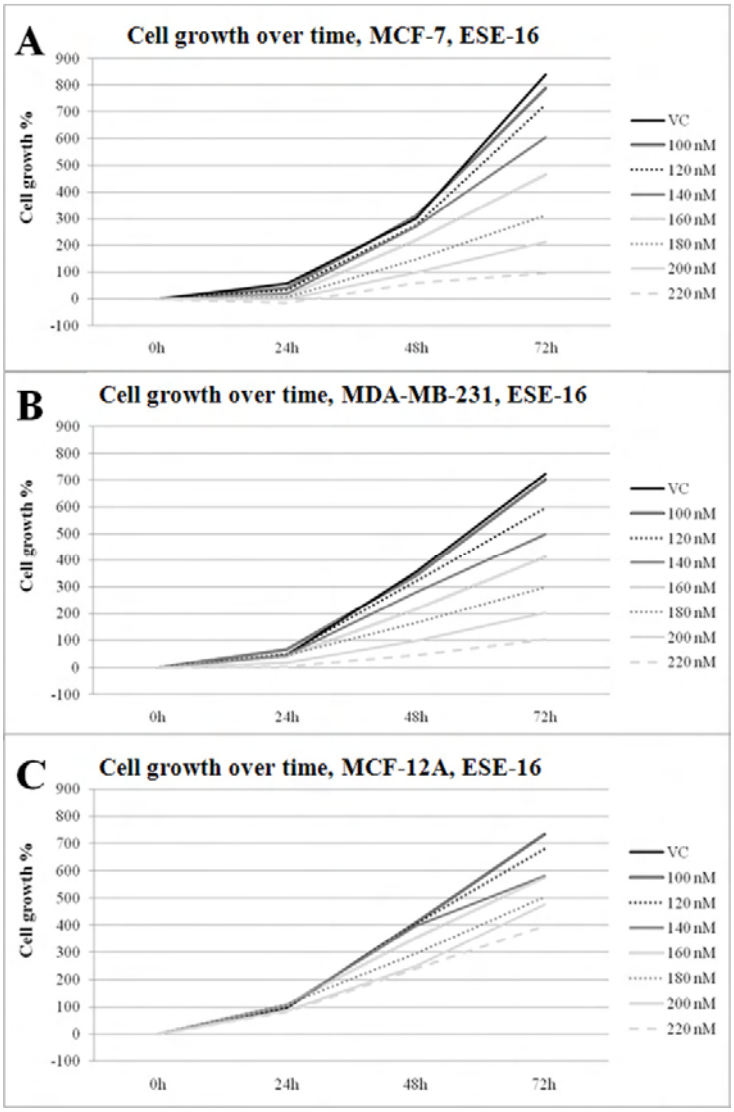

Figure 3.9: Cell growth curves over 72 h exposure for ESE-16 on MCF-7, MDA-MB-231 and MCF-12A cells. ESE-16 inhibited cell growth in a dose-dependent manner in the different cell lines.

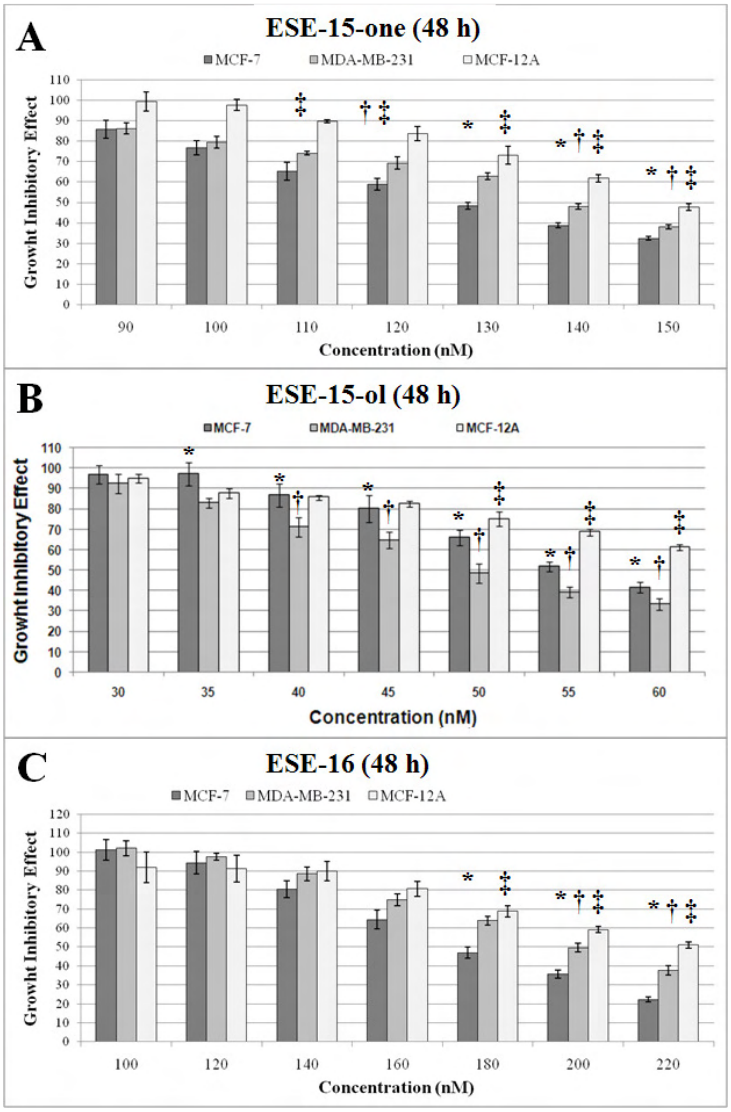

Figure 3.10: Cell numbers expressed as a percentage of cells relative to 100% control after exposure to different concentrations of ESE-15-one, ESE-15-ol and ESE-16.For ESE-15-one the GI_{50} was calculated at 130 nM (A), 140 nM (B) and 150 nM (C) for MCF-7, MDA-MB-231 and MCF-12A cells respectively. The GI_{50} for ESE-15-olwas calculated at 50 nM for MCF-7 (A) and MDA-MB-231 (B) cells and > 60 nM for MCF-12A (C) cells. For ESE-16 the GI_{50} was calculated at 200 nM for MCF-7 (A) and MDA-MB-231 (B) and 220 nM for MCF-12A cells (C)

* indicates a *P*-value < 0.05 for growth inhibition between MCF-7 and MDA-MB-231 cells.

† indicates a *P*-value < 0.05 for growth inhibition between MDA-MB-231 and MCF-12A cells.

‡ indicates a *P*-value < 0.05 for growth inhibition between MCF-12A and MCF-7 cells.

Spectrophotometry: Cell cytotoxicity

Quantification of plasma membranedamage gives an indication of cell viability (208). LDH is present in all cell types and is rapidly released into the cell culture medium upon damage of the plasma membrane(208). A lactate dehydrogenase colorimetric assay was utilized to measure the ability of extracellular LDH to oxidize lactate to reduce NAD)to reduced nicotinamide adenine dinucleotide (NADH). The LDH cytotoxicity assay kit utilizes WST-8 to react with NADH produced by lactate from LDH. The intensityof the generated color correlates directly amount of released LDH as a result of a damaged the plasma membrane. Time-dependent studies were conducted at intervals of 24 h and 48 h using the GI_{50} concentration of each compound for the MDA-MB-231 (140 nM for ESE-15-one, 50 nM for ESE-15-ol and 200 nM for ESE-16) cells. The MDA-MB-231 cell line is a metastatic cell line that constitutively express CAIX mRNA and has been shown to express CAIX protein under hypoxic conditions (276). Therefore, using the GI_{50} for the metastatic MDA-MB-231 cells as a reference concentration allows us to compare the relative sensitivity of tumorigenic but not metastatic MCF-7 cells and non-tumorigeneic MCF-12A cells to the MDA-MB-231 cells.

Exponentially growing MCF-7, MDA-MB-231 and MCF-12A cells were seeded in 96-well tissue culture plates at a cell density of 5000 cells per well. Cells were incubated at 37 °C for 24 h to allow for attachment. After 24 h attachment the medium were discarded and the cells were exposed to the desired concentrations of the newly synthesized compounds, as well as the vehicle control (DMSO at 0.01% v/v). Background-controls were be included by adding only growth medium to the plates in order to subtract the effects that the medium has on the assay itself. The vehicle-treated controls, background-controls and compound-treated cells were incubated for 24 h and 48 h before the assay was performed.

A positive control for LDH production by each cell line was included by adding 10 µl of lysis buffer 30 min before the end of the 24 h and 48 h exposure times. After the 24 h and 48 h exposure, 10 µl of each sample was transferred to a new plate and incubated for 30 min at room temperature with the WST-8 reagent. The absorbance was read at 450 nm with 630 nm as

reference with an EL_x800 Universal Microplate Reader from Bio-Tek Instruments Inc. (Vermont, United States of America).

The cytotoxicity will be calculated as follows:

$$Cytoxicity\ (\%) = \frac{TS - BC}{PC - BC} * 100$$

TS = Test Sample
BC = Background Control
PC = Positive Control

Cytotoxicity after 24 h and 48 h increased in all cell lines for all treatments and all three cell lines (Figure 3.11). ESE-16 was the most cytotoxic of the tested compounds and ESE-15-ol the least (Figure 3.11). MCF-12A cells where the least affected when compared to the MCF-7 and MDA-MB-231 cells for the corresponding compounds after 48 h exposure (Figure 3.11). For example, in ESE-15-one- treated cells after 48 h exposure there was a more than two-fold increase in cytotoxicity in MCF-7 (33.6%) and MDA-MB-231 (31.9%) cells when compared to MCF-12A (14.5%) cells (Figure 3.11 B). In ESE-15-ol- treated cells after 48 h exposure, cytotoxicity in MCF-7 (25.5%) and MDA-MB-231 (26.7%) cells were statistically significantly more than the MCF-12A (12.8%) cells (Figure 3.11 B). The cytotoxicity of MCF-12A (27%) cells in ESE-16-treated cells after 48 h exposure was statistically significantly less than MCF-7 (41.9%) and MDA-MB-231 (37.6%) cells (Figure 3.11 B).

Cytotoxicity also increased by at least two-fold from 24 h to 48 h in all treated samples (Figure 3.11 A vs B and Table 3.11). Together these results indicate that the non-tumourigenic MCF-12A cell line was the least affected by cellular toxicity when treated with the antimitotic compounds. Also, the compounds do not appear to decrease their cytotoxic effect over time.

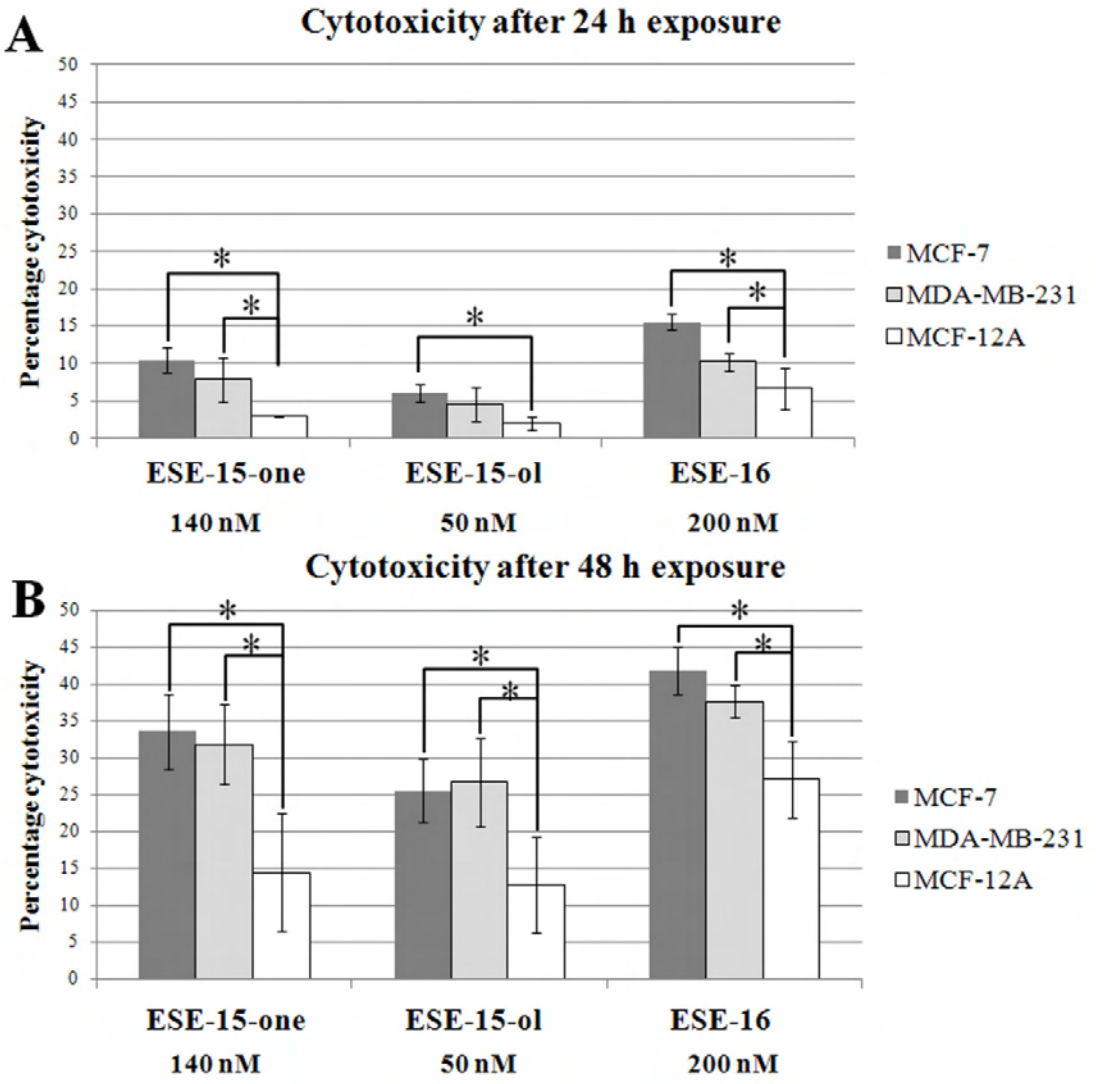

Figure 3.11: Cytotoxicity MCF-7, MDA-MB-231and MCF-12A cells exposed to ESE-15-one, ESE-15-ol and ESE-16 for 24 h and 48 h.Cytotoxicity increased in all cell lines for all treatments and all three cell lines. ESE-16 was the most cytotoxic of the tested compounds and ESE-15-ol the least (A and B). MCF-12A cells where the least affected when compared to the MCF-7 and MDA-MB-231 cells for the corresponding compounds after 48 h exposure (B).

Table 3.11: Fold increase in cytotoxicity from 24 h to 48 h. Increase in cytotoxicity in MCF-7, MDA-MB-231and MCF-12A cells exposed to ESE-15-one, ESE-15-ol and ESE-16. Cytotoxicity from 24 h to 48 h increased in all treated samples.

	ESE-15-one (150 nM)	**ESE-15-ol (50 nM)**	**ESE-16 (200 nM)**
MCF-7	3.22	4.29	2.71
MDA-MB-231	4.06	5.82	3.71
MCF-12A	4.89	3.54	3.42

Real-time Cell Growth Analysis: xCELLigence Real-Time Cell Analyzer

The xCELLigence System (Real-Time Cell Analyzer Single Plate (RTCA SP®) system) from RocheDiagnostics GmbH (Roche Applied Science, 68298 Mannheim, Germany) measured the real-time proliferation of MCF-7, MDA-MB-231 and MCF-12A cells over a period of 48 h after exposure to ESE-16 at 200 nM. The Cell Index was normalized to 1 at beginning of exposure time, 24 hours after seeding in order to compare cells growth of the different cell lines. The cell growth curves indicate that MCF-12A cells were the least affected by ESE-16, confirming the results for the crystal violet and cytotoxicity assays (Figure 3.12). Also, the characteristic "spoon-shaped" curve observed in MCF-7 and MDA-MB-231 cells indicate that cells react to ESE-16 similar to other antimitotic compounds(277).

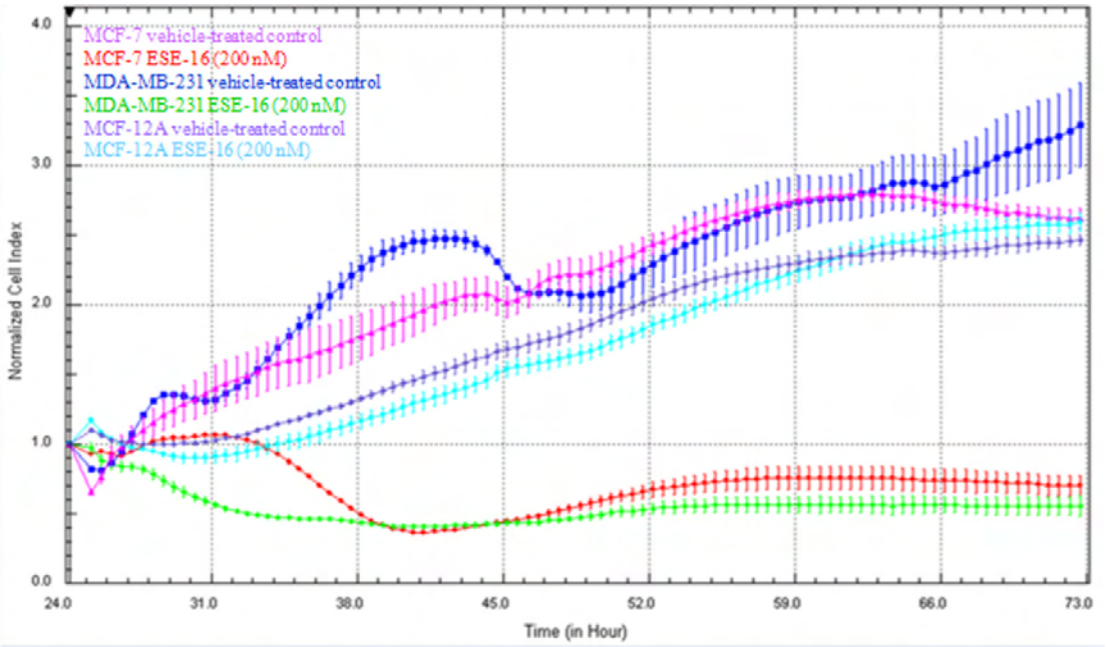

Figure 3.12: Real-time dynamic monitoring of cell adhesion and proliferation via the xCELLigence system ESE-16-treated cells.MCF-7 (red) and MDA-MB-231 (green) cell growth was negatively affected when compared to the vehicle-treated control while MCF-12A-treated cells showed little divergence form the vehicle-treated control.